

# DeTEC: Detection of Touching Elongated Cells in SEM Images

A. Memariani<sup>1(✉)</sup>, C. Nikou<sup>1</sup>, B.T. Endres<sup>2</sup>, E. Bassères<sup>2</sup>, K.W. Garey<sup>2</sup>, and I.A. Kakadiaris<sup>1</sup>

<sup>1</sup> Computational Biomedicine Lab, Department of Computer Science,  
University of Houston, Houston, TX, USA

{amemaria, cnikou, ikakadia}@central.uh.edu

<sup>2</sup> Department of Pharmacy Practice and Translational Research,  
University of Houston, Houston, TX, USA  
{btendres, ebassere, kgarey}@central.uh.edu

**Abstract.** A probabilistic framework using two random fields, DeTEC (Detection of Touching Elongated Cells) is proposed to detect cells in scanning electron microscopy images with inhomogeneous illumination. The first random field provides a binary segmentation of the image to superpixels that are candidates belonging to cells, and to superpixels that are part of the background, by imposing a prior on the smoothness of the texture features. The second random field selects the superpixels whose boundaries are more likely to form elongated cell walls by imposing a smoothness prior onto the orientations of the boundaries. The method is evaluated on a dataset of *Clostridium difficile* cell images and is compared to CellDetect.

## 1 Introduction

Cell detection is an important task in the analysis of microscopy images, with many applications such as cell counting, quantification of cell wall integrity, and deformation quantification. Despite the advances in scanning electron microscopy (SEM), the acquired cell images are often noisy with low contrast. In addition, inhomogeneously illuminated cells of various sizes may be touching, making the detection of micron scale cells a challenging task. Standard methods such as ellipse fitting and Hough transform [1] fail to detect cells in these types of images due to the their challenging nature.

Recent computer vision methods in cell detection fall into three categories. The first category assumes that cells differ significantly from their background. A machine learning algorithm such as random forests [2] assigns a score to pixels based on features extracted from a local neighborhood. Local extremum points of the scores represent the cell centroids [3–6]. Other approaches define the score based on the distance of each point to the nearest annotated cell centroid [2]. The second category includes methods that learn a mapping from global or local appearances to a real-value [7–9]. These methods are sensitive to the density of the cells in the image. Furthermore, their main focus is to count the number of

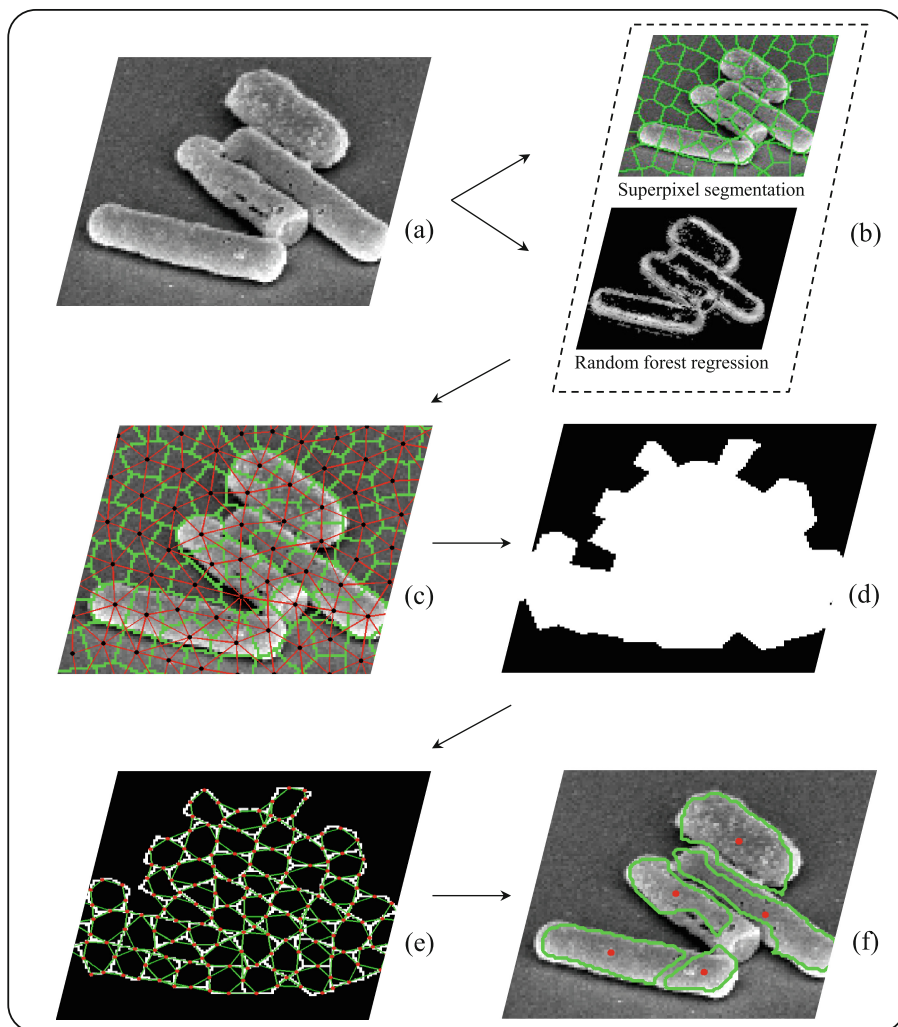


**Fig. 1.** Overview of the method (the figure is best viewed in color). (a) Depiction of a cell cluster in the original image. (b) Depiction of superpixel map (Top), and cell wall probabilities predicted by random forest regression (Bottom). (c) A random field defined over the superpixels provides potential cell regions (the nodes are represented by black dots and the edges by red lines). (d) Depiction of output superpixel area provided by the random field in (c). (e) A second random field defined over the remaining superpixel boundaries detects elongated cells (the nodes are represented by red dots and the edges by green lines). (f) Depiction of detected centroids (red), and cell walls (green). (Color figure online)

**Algorithm 1.** DeTEC algorithm.

---

**Input** : Original image, trained random forest for cell wall probability estimation

**Output:** Cell centroids

- 1 Compute the superpixel map.
- 2 Compute the cell wall probability map.
- 3 **begin** First MRF: Cell candidate detection
- 4   For every superpixel  $i$  ( $i = 1, \dots, n^1$ ), compute the feature vector  $\mathbf{f}_i^1$ .
- 5   Apply Gaussian mixture model on  $\mathbf{f}^1$  to compute parameter set  $\mathcal{T}$ .
- 6   For every superpixel  $i$  compute the unary potentials as the negative log of the Gaussian probability densities with parameter  $\mathcal{T}$ .
- 7   Apply graph cut to find the set of superpixel labels  $\mathcal{L}^1$  that minimizes  $E^1(\mathcal{L}^1)$ .
- 8   For every superpixel  $i$  selected in  $\mathcal{L}^1$  record the indexes of the superpixel boundary segments  $b_{ij}$  in the adjacency matrix,  $j \in \mathcal{G}_i^1$ .
- 9 **end**
- 10 **begin** Second MRF: Elongated cell separation
- 11   For every superpixel boundary segment  $q$  ( $q = 1, \dots, n_2^2$ ), selected by the first MRF compute the feature vector  $\mathbf{f}_q^2$ .
- 12   Apply Gaussian mixture model on  $\mathbf{f}^2$  to compute parameter set  $\mathcal{O}$ .
- 13   For every superpixel boundary segment  $q$  compute unary potentials as the negative log of the Gaussian mixture model with parameter set  $\mathcal{O}$ .
- 14   Apply graph cut to find the set of boundary segment labels  $\mathcal{L}^2$  that minimizes  $E^2(\mathcal{L}^2)$ .
- 15   Generate morphological connected components using the contours of the selected superpixel boundary segments.
- 16   Compute the centroids of the remaining connected components.
- 17 **end**

---

cells rather than the localization of cells. The third category are the region-based methods, where potential cell regions are first detected. Then, an optimization algorithm selects the best candidates based on statistical texture and appearances [10–15] or correlation clustering [16].

We propose a method capable of detecting touching and inhomogeneously illuminated cells (Fig. 1). Our contributions are the following:

- We propose two random fields, combining texture and shape information to detect elongated structures.
- We impose smoothness to the orientation between the segments of a contour to estimate the cell wall of elongated cells.
- We introduce a new dataset of *Clostridium difficile* cells obtained by SEM which is used for the evaluation of the method.

The rest of the paper is organized as follows: Sect. 2 describes DeTEC. Section 3 discusses the experimental results, including comparison with CellDetect [12].

## 2 Two Random Fields for Elongated Cell Detection

As a pre-processing stage, we apply a random forest regression to estimate the probability of a pixel belonging to a cell wall (Fig. 1(b), bottom). To train the random forest, we compute a feature vector containing a set of rotation invariant local binary patterns (LBP) [17], the response of the images to difference of Gaussians of varying width ratios, and to a vessel enhancement filter [18] (Fig. 1(b), bottom). Six images were manually annotated to provide the labels for training the random forest.

The next step involves developing a method based on two random fields: the first random field imposes texture smoothness while the second random field imposes smoothness on the continuity of superpixel boundary segments. At first, a cell image is divided into superpixels [19] and an MRF separates the cells from the background at superpixel level. However, a standard MRF may not separate clustered cells.

Cell walls have a key role in the detection of cells and the separation of adjacent cells. Every superpixel boundary segment has a likelihood of belonging to a cell wall. Moreover, neighboring superpixel boundary segments are more likely to have a small variance in orientation if they form an elongated cell wall. These two observations are key-issues in the proposed cell detection method.

**Cell Candidate Detection:** The first random field is imposed onto the superpixels adjacency graph (Fig. 1(c)). A graph cut provides a binary segmentation of superpixels with the following objective function:

$$E^1 = \sum_i u_i^1(\mathbf{f}_i^1 | \mathcal{L}^1, \mathcal{T}) + \sum_i \sum_{j \in \mathcal{G}_i^1} v_{i,j}^1(l_i^1, l_j^1), \quad (1)$$

where the first term is the sum of unary potentials  $u_i^1$ , consisting of a mixture of two Gaussians with parameter set  $\mathcal{T} = \{\theta_0, \theta_1\}$ , modeling the foreground and the background with superpixel label set  $\mathcal{L}^1 = \{l_i^1 \in \{0, 1\} | i = 1, \dots, n_s\}$ . The feature vector  $\mathbf{f}_i^1$  comprises a vector of orientation invariant LBPs, along with the mean, median, and standard deviation of pixels belonging to the  $i^{\text{th}}$  superpixel. The second term is the pairwise potential where  $\mathcal{G}_i^1$  is the set of superpixel neighbors of the  $i^{\text{th}}$  superpixel.

In the standard MRF formulation, the pairwise term enforces the superpixels to have the same labels as their neighbors. However, when two cells are close to each other but not touching (e.g., they are separated by a small number of background pixels), the pairwise term forces the small background region between the two cells to be labeled as part of a cell. To avoid these false positives, we define a new pairwise penalty involving the probability of the boundary separating neighboring superpixels to be part of a cell wall [20, 21]. Therefore, we define the pairwise potential between neighboring superpixel labels  $l_i^1$  and  $l_j^1$  by:

$$v_{i,j}^1(l_i^1, l_j^1) = \begin{cases} -\log(\pi_{ij}^1), & \text{if } l_i^1 \neq l_j^1, \\ 0, & \text{if } l_i^1 = l_j^1, \end{cases} \quad (2)$$

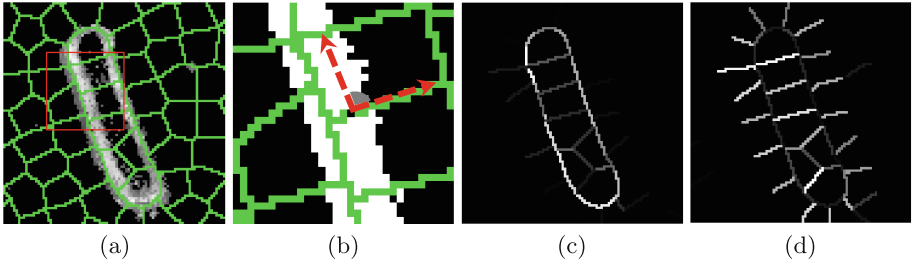


**Fig. 2.** (a) Depiction of the superpixel map (green) is overlaid onto the cell wall probability map. (b) Zoomed visualization of the area inside the red square in (a). The gray angle is between the largest connected component in the probability map (white) and the superpixel boundary segments (green). (c) The mean cell wall probabilities  $\pi_{ij}^1$  of the image depicted in (a). (d) Depiction of the standard deviations of cell wall probabilities. (a) Depiction of the superpixel map (green) is overlaid onto the cell wall probability map. (b) Zoomed visualization of the area inside the red square in (a). The gray angle is between the largest connected component in the probability map (white) and the superpixel boundary segments (green). (c) The mean cell wall probabilities  $\pi_{ij}^1$  of the image depicted in (a). (d) Depiction of the standard deviations of cell wall probabilities. (Color figure online)

where  $\pi_{ij}^1$  is the probability indicating whether the boundary between the  $i^{\text{th}}$  and  $j^{\text{th}}$  superpixels is on a cell wall:

$$\pi_{ij}^1 = \frac{1}{|\mathcal{N}_{ij}|} \sum_{x \in \mathcal{N}_{ij}} p_x \cdot \cos \alpha_{ij}, \quad (3)$$

where  $\mathcal{N}_{ij}$  is the set of all pixels at the border of the two superpixels indexed by  $i$  and  $j$ , and  $p_x$  is the probability of a pixel  $x$  belonging to a cell wall. This value is obtained from the random forest (Fig. 1(b), bottom).

In Eq. (3)  $\alpha_{ij}$  is the angle between the superpixel boundary component and the corresponding connected component in the probability map in a neighborhood around position  $x$  (Fig. 2(b)). Thus, a superpixel boundary receives a high cell wall score when it is parallel to a real cell wall. If the boundary segment is more likely to be part of a cell wall, then the two touching superpixels are less likely to have the same labels.

This MRF model segments the cell regions from the background (Fig. 1(d)). However, when the cells are clumped together, every cluster of cells is segmented as one connected component. The second MRF takes the boundary segments of the cell superpixels and detects a set of boundary components that are more likely to form an elongated cell wall to detect elongated cells and separate the clustered cells. The second random field considers only the selected candidate superpixels. Therefore, the number of boundary segments in the second layer is much smaller than the total number of boundary segments in the original superpixel map.

**Elongated Cell Separation:** The second random field is defined over the superpixel boundary segments selected by the first random field. The objective of this step is to cluster these boundaries into two categories: boundaries that belong to elongated cell walls, and the rest of the boundaries. The energy function to be minimized is:

$$E^2 = \sum_q u_q^2(\mathbf{f}_q^2 | \mathcal{L}^2, \mathcal{O}) + \sum_q \sum_{r \in \mathcal{G}_q^2} v_{q,r}^2(l_q^2, l_r^2). \quad (4)$$

The unary term represents the potential of the superpixel boundary component to be part of a cell wall. Similar to the first layer,  $u_q^2$  is modeled by a Gaussian mixture model parameterized by  $\mathcal{O}$  and  $\mathcal{L}^2 = \{l_q^2 \in \{0, 1\} | q = 1, \dots, n_2^2\}$ . The feature vector  $\mathbf{f}_q^2$  comprises the mean  $\pi_{ij}^2$  (defined similarly as  $\pi_{ij}^1$  in Eq. (3)) and the standard deviation of the cell wall probabilities for the  $q^{\text{th}}$  superpixel boundary components (Fig. 2). The second term models the pairwise potential enforcing the elongation of the  $q^{\text{th}}$  boundary segment with respect to its neighbors in  $\mathcal{G}_q^2$ :

$$v_{q,r}^2(l_q^2, l_r^2) = \begin{cases} \cos(\beta_{qr}) & \text{if } l_q^2 \neq l_r^2 \\ 0 & \text{if } l_q^2 = l_r^2 \end{cases}, \quad (5)$$

where  $\beta_{qr}$  is the angle between superpixel boundary segments  $q$  and  $r$ , and is computed by taking the minimum angle between the estimated orientations of  $q$  and  $r$ . When two adjacent boundary components have different orientations, they are less likely to have the same label. The extracted superpixel boundary components form the detected cell walls that separate the cell regions (Fig. 1(f)).

### 3 Experimental Results

To evaluate our method, we employed a dataset containing 7 *Clostridium difficile* cell images with a total of 78 cells acquired via SEM imaging with 10000X magnification and resolution of  $411 \times 712$  pixels. The images have low cell densities but many cells are clustered together, making detection challenging. Furthermore, cells areas are highly inhomogeneously illuminated. This holds not only between cells but mainly for pixels belonging to the same cell (Fig. 4). In some cases, the cells are partially destroyed due to the biological treatment.

**Table 1.** Parameter settings used in DeTEC.

Parameter(s)	Value(s)
DoG standard deviations	$\sigma_1 = 1$ , and $\sigma_2 \in \{5, 10\}$
Vessel enhancement filter [18] parameters	Scale range = [1, 8], $\beta_1 = 0.5$ , $\beta_2 = 15$ , and Scale ratio = 2
Distance from ground truth for true positives ( $d$ )	20 pixels

**Table 2.** Comparative results between DeTEC, CellDetect, and CellDetect\*. In CellDetect\*, a cluster of cells detected as one cell is considered a true positive.

Method	Precision	Recall	F-score
CellDetect [12]	0.53	0.27	0.36
CellDetect* [12]	0.95	0.57	0.71
DeTEC	0.69	0.93	<b>0.79</b>

Cell centroids are manually annotated to establish the ground truth. A centroid is considered to be detected if it lies within a distance  $d$  from an annotated centroid. The distance is defined based on the length of the major axis of the smallest cell in the dataset. False positives are defined accordingly. We used the F-score for comparison.

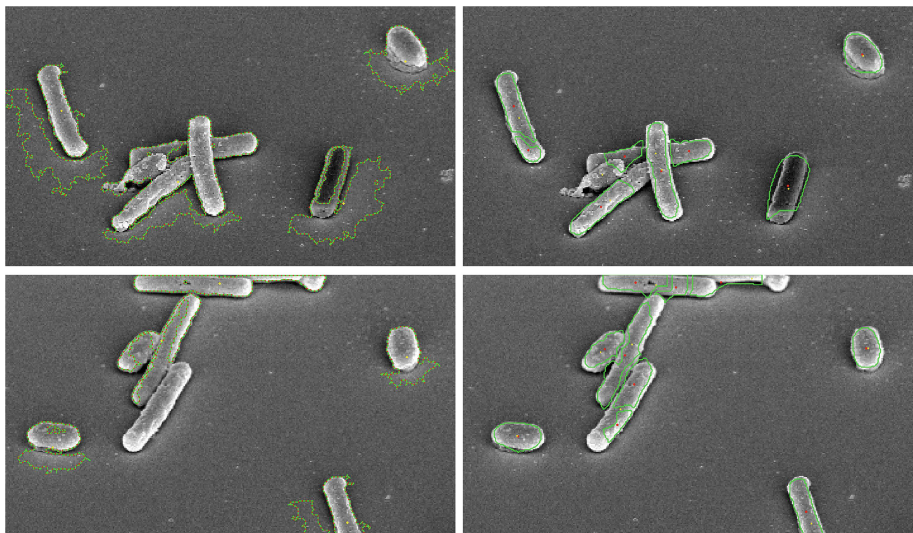
Table 1 depicts the parameter settings for DeTEC. We compared the result with CellDetect [12], which is a supervised region-based cell detection method. CellDetect uses extremal regions [22] to detect candidate cell regions. Then, a statistical model of the cell appearance evaluates the selected extremal regions. The training and testing for CellDetect was based on a leave-one-out cross validation. In many cases, CellDetect fails to separate touching cells. Therefore, we considered two experiments for the comparison. The first experiment evaluates the detection of individual cells. The second experiment, which is strongly favorable to CellDetect, considers the attached cells as one object. In that case, detected clustered cells would be considered true positives even if CellDetect indicates the whole cluster as one cell.

Table 2 summarizes the performance of DeTEC against the two mentioned experiments. As may be observed, DeTEC achieves a higher F-score even in the case where detected clustered cells are considered as true positives for CellDetect. Accepting clustered cells improves the precision of CellDetect significantly. However, CellDetect fails to detect some cells due to the assumption of existing extremal regions that can represent the cells [15].

Figure 3 depicts representative examples of CellDetect and the DeTEC. The detected boundaries for an out-of-focus cell may not match the exact cell wall (Fig. 3(c)) since superpixel boundaries may not fit the cell wall line due to poor illumination. However, DeTEC could successfully estimate the centroid since we employed the cell wall probabilities from a small neighborhood around the superpixel boundaries.

DeTEC has a significantly higher F-score with respect to CellDetect [12]. This is also true for its precision and recall values. It seems that precision could have been better. However, this is due to the multiple cell centroids it detects in the case of overlapping cells or cells having undergone a biological treatment (3).

Finally, Fig. 4 depicts samples of detected inhomogeneously illuminated cells despite shadows and artifacts. Inhomogeneous illumination may cause the first random field to include the superpixels around the cells in the segmentation due to shadows and artifacts. However, the second random field examines whether the selected superpixel boundary segments are likely to form a cell wall with their neighbors, and eventually rejects them.



**Fig. 3.** Detected centroids and boundaries for CellDetect [12] (Left), and the DeTEC (Right). For DeTEC, annotated and detected centroids are shown in yellow and red, respectively. (Color figure online)

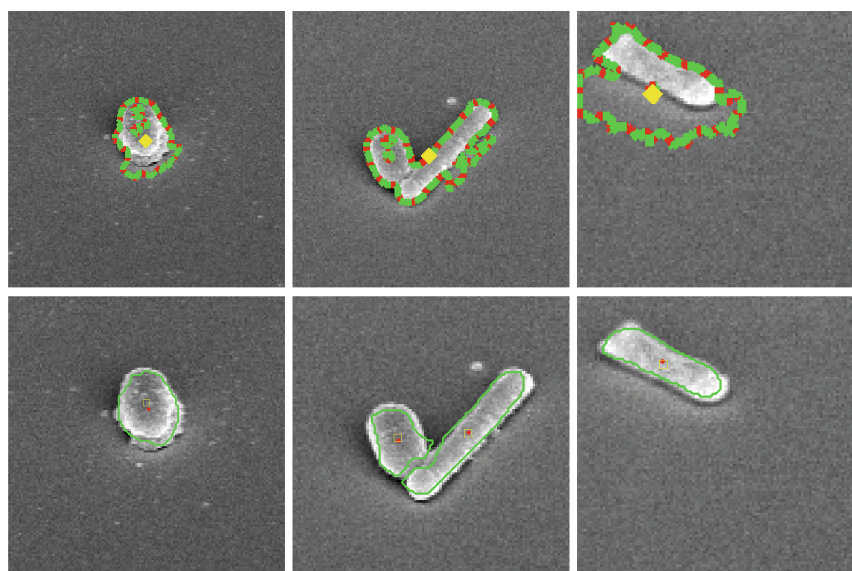


**Fig. 4.** Inhomogeneous illumination creates shadows on the cell surface and a bright area around the cell. Detected centroids for CellDetect [12] is shown (Top row). Detected and true centroids for DeTEC are shown as squares and circles, respectively (Bottom row).

## 4 Conclusion

We proposed a method with two random fields to detect elongated cells in SEM images that is robust for detecting inhomogeneously illuminated cells. The detection process is automatic, robust to inhomogeneous illumination, and suitable for the analysis of high-throughput microscopy images. The method successfully separates touching cells by estimating their cell walls. In general, our method has better overall performance than CellDetect.

In this work, we did not consider the case of cross-overlapping cells, which has been previously addressed by post-processing [6], deformable models [23], or watersheds [24]. Our detection method was implemented using a graph cut algorithm. However, the idea could be further extended to employ a supervised approach such as conditional random fields.

**Acknowledgments.** This work was supported in part by the Texas Department of State Health Services (Grant #2015-046620) and by the Hugh Roy and Lillie Cullen Endowment Fund.

## References

1. Vedaldi, A., Fulkerson, B.: VLFeat: an open and portable library of computer vision algorithms. In: Proceedings of 18th ACM International Conference on Multimedia, Florence, Italy, pp. 1469–1472 (2010)
2. Kainz, P.: You should use regression to detect cells. In: Proceedings of Medical Image Computing and Computer-Assisted Intervention, Munich, pp. 276–283 (2015)
3. Minaee, S., Fotouhi, M., Khalaj, B.: A geometric approach to fully automatic chromosome segmentation. In: Proceedings of IEEE Signal Processing in Medicine and Biology Symposium, Philadelphia, PA, pp. 1–6 (2014)
4. Wu, B., Nevatia, R.: Detection and segmentation of multiple, partially occluded objects by grouping, merging, assigning part detection responses. *Int. J. Comput. Vision* **82**, 185–204 (2009)
5. Wayalun, P., Chomphuwiset, P., Laopracha, N., Wanchanthuek, P.: Images enhancement of G-band chromosome using histogram equalization, OTSU thresholding, morphological dilation and flood fill techniques. In: Proceedings 8th International Conference on Computing and Networking Technology, Gueongju, China, pp. 163–168 (2012)
6. Saiyod, S., Wayalun, P.: A hybrid technique for overlapped chromosome segmentation of G-band mataspread images automatic. In: Proceedings of 4th International Conference on Digital Information and Communication Technology and its Applications, Bangkok, Thailand, pp. 400–404 (2014)
7. Lempitsky, V., Zisserman, A.: Learning to count objects in images. In: Advances in Neural Information Processing Systems, Vancouver, Canada, pp. 1324–1332 (2010)
8. Fiaschi, L., Koethe, U., Nair, R., Hamprecht, F.A.: Learning to count with regression forest and structured labels. In: Proceedings of 21st International Conference on Pattern Recognition, Tsukuba, Japan, pp. 2685–2688 (2012)
9. Foroughi, H., Ray, N., Zhang, H.: Robust people counting using sparse representation and random projection. *Pattern Recogn.* **48**, 3038–3052 (2015)

10. Daněk, O., Matula, P., Ortiz-de Solórzano, C., Muñoz-Barrutia, A., Maška, M., Kozubek, M.: Segmentation of touching cell nuclei using a two-stage graph cut model. In: Proceedings of Scandinavian Conference on Image Analysis, Oslo, Norway, pp. 410–419 (2009)
11. Keuper, M., Schmidt, T., Rodriguez-Franco, M., Schamel, W., Brox, T., Burkhardt, H., Ronneberger, O.: Hierarchical markov random fields for mast cell segmentation in electron microscopic recordings. In: Proceedings of IEEE International Symposium on Biomedical Imaging: From Nano to Macro, Chicago, pp. 973–978 (2011)
12. Arteta, C., Lempitsky, V., Noble, J.A., Zisserman, A.: Learning to detect cells using non-overlapping extremal regions. In: Proceedings of International Conference on Medical Image Computing and Computer-Assisted Intervention, Nice, France, pp. 348–356 (2012)
13. Arteta, C., Lempitsky, V., Noble, J.A., Zisserman, A.: Learning to detect partially overlapping instances. In: Proceedings of IEEE Conference on Computer Vision and Pattern Recognition, Portland, OR, pp. 3230–3237 (2013)
14. Santamaria-Pang, A., Rittscher, J., Gerdes, M., Padfield, D.: Cell segmentation and classification by hierarchical supervised shape ranking. In: Proceedings of IEEE International Symposium on Biomedical Imaging, Brooklyn, NY, pp. 1296–1299 (2015)
15. Arteta, C., Lempitsky, V., Noble, J.A., Zisserman, A.: Detecting overlapping instances in microscopy images using extremal region trees. *Med. Image Anal.* **27**, 3–16 (2016)
16. Zhang, C., Yarkony, J., Hamprecht, F.A.: Cell detection and segmentation using correlation clustering. In: Proceedings of Medical Image Computing and Computer-Assisted Intervention, Boston, MA, pp. 9–16 (2014)
17. Ojala, T., Pietikainen, M., Maenpaa, T.: Multiresolution gray-scale and rotation invariant texture classification with local binary patterns. *IEEE Trans. Pattern Anal. Mach. Intell.* **24**, 971–987 (2002)
18. Frangi, A.F., Niessen, W.J., Vincken, K.L., Viergever, M.A.: Multiscale vessel enhancement filtering. In: International Conference on Medical Image Computing and Computer-Assisted Intervention, Cambridge, MA, pp. 130–137 (1998)
19. Mori, G.: Guiding model search using segmentation. In: Proceedings of 10th IEEE International Conference on Computer Vision, Beijing, China, vol. 1, pp. 1417–1423 (2005)
20. Andres, B., Kappes, J.H., Beier, T., Kothe, U., Hamprecht, F.A.: Probabilistic image segmentation with closedness constraints. In: Proceedings of International Conference on Computer Vision, Barcelona, Spain, pp. 2611–2618 (2011)
21. Yarkony, J., Ihler, A., Fowlkes, C.C.: Fast planar correlation clustering for image segmentation. In: Proceedings of European Conference on Computer Vision, Florence, Italy, pp. 568–581 (2012)
22. Matas, J., Chum, O., Urban, M., Pajdla, T.: Robust wide-baseline stereo from maximally stable extremal regions. *Image Vis. Comput.* **22**, 761–767 (2004)
23. Plissiti, M.E., Nikou, C.: Overlapping cell nuclei segmentation using a spatially adaptive active physical model. *IEEE Trans. Image Process.* **21**, 4568–4580 (2012)
24. Karvelis, P., Likas, A., Fotiadis, D.I.: Identifying touching and overlapping chromosomes using the watershed transform and gradient paths. *Pattern Recogn. Lett.* **31**, 2474–2488 (2010)